Nanoscale Research Letters
a SpringerOpen Journal

NANO EXPRESS Open Access

# Controllable synthesis of $MnO_2$/polyaniline nanocomposite and its electrochemical capacitive property

Fanhui Meng[1,2], Xiuling Yan[1,3], Ye Zhu[2] and Pengchao Si[1*]

**Abstract**

Polyaniline (PANI) and $MnO_2$/PANI composites are simply fabricated by one-step interfacial polymerization. The morphologies and components of $MnO_2$/PANI composites are modulated by changing the pH of the solution. Formation procedure and capacitive property of the products are investigated by XRD, FTIR, TEM, and electrochemical techniques. We demonstrate that $MnO_2$ as an intermedia material plays a key role in the formation of sample structures. The $MnO_2$/PANI composites exhibit good cycling stability as well as a high capacitance close to 207 F $g^{-1}$. Samples fabricated with the facile one-step method are also expected to be adopted in other field such as catalysis, lithium ion battery, and biosensor.

**Keywords:** Interfacial synthesis, Polyaniline, $MnO_2$, Composite, Electrochemical capacitor

## Background

As a sort of classic conducting materials, polyaniline (PANI) possesses good conductivity with specific organic characters that metal cannot match, which has attracted a lot of attentions for its wide applications in capacitance, sensors, ultrafast nonvolatile memory devices, and chemical catalysis [1-5]. $MnO_2$ has been widely studied as a promising environmentally benign transition metal oxide for sensor, catalyst, lithium battery, and electrochemical capacitor [6-9]. In the quest for superior performance, aniline has been polymerized in combining with other materials to obtain a promising performance, in which PANI/graphene, PANI/carbon nanotube, PANI/Au electrode, and others have been successfully synthesized [1,2,10]. Meanwhile, hybrid composites consisted of $MnO_2$, and other materials have also been fabricated to improve their behaviors in battery or supercapacitor [11-15]. In particular, the structures of $MnO_2$/PANI have been constructed with different methods, and the synergistic effect of $MnO_2$ and PANI has been demonstrated in supercapacitor and catalysis toward $H_2O_2$ oxidation or organic dyes [16-20]. Considering the catalyst-size dependent reaction selectivity and agglomeration involved in nanostructures and specific nanoscale architecture, the big challenge for high-efficiency and outstanding features is still the controllable synthesis of uniform structures [21,22].

With respect to PANI synthesis, chemical and physical methods have been recommended [5,23-31], in which the facile interfacial polymerization is a highly flexible approach without any templates [3,23,24]. The oxidant and reducing agent are separated in the aqueous and organic solutions, while the redox reaction can occur at the interface. As far as the products are removed into the bulk solution, new polymerization can happen at the interface while secondary growth of PANI are prevented, in which both the shape and size of the products can be controlled. In addition, synthesis of $MnO_2$ via reducing the compounds containing $MnO_4^-$ and $MnO_4^{2-}$ has been extensively used due to its simpleness and low cost. During that procedure, the pH of $KMnO_4$ solution plays a critical role in the intermediate oxidation state and finally the products:

$$MnO_4^- + 2H_2O + 3e = MnO_2(s) + 4OH^- \quad (1)$$

$$MnO_4^- + 8H^+ + 5e = Mn^{2+} + 4H_2O \quad (2)$$

At a high pH, $MnO_2$ is the main product while $Mn^{2+}$ is the final product at a low pH.

* Correspondence: PCSi@sdu.edu.cn
[1]Key Laboratory for Liquid–solid Structural Evolution and Processing of Materials, Ministry of Education, School of Materials Science and Engineering, Shandong University, Jinan 250061, People's Republic of China
Full list of author information is available at the end of the article

Recently, due to the depleting of fossil fuels and the severe environmental problems caused by burning fossil fuels, supercapacitors with large-power density and long-time cycling have attracted attentions of many researchers [25,26]. As low-cost and easily obtained materials, the capacitive properties of $MnO_2$, PANI, and $MnO_2$/PANI composites have been widely studied [27-29].

In this work, we utilize the above mechanism to deliberately synthesize a series of $MnO_2$/PANI composites with controllable morphology and uniform size by means of the interfacial polymerization and adjusting the pH of solutions. In the synthesis, monomer aniline and $KMnO_4$ are used as reducing agent in organic solution and oxidant in aqueous solution, respectively. PANI and $MnO_2$/PANI are prone to diffusing into the aqueous phase because they are hydrophilic in the doped salt forms [3,23,24]. In the composite, PANI is expected to allow uniform $MnO_2$ particle dispersion and convenient electron transfer. In the present study, the formation mechanism and the electrochemical capacitive performance of the composites have been investigated.

## Methods

### Preparation of $MnO_2$/PANI

Aniline was firstly distilled under reduced pressure. Then, 0.6 mL of aniline was dissolved in benzene (10 mL) solution, while 0.2 g of $KMnO_4$ was dissolved in the solution (20 mL) with 1 M $ClO_4^-$ as the doping anion (we used $HClO_4$ as the source of $ClO_4^-$). The organic solution was added into aqueous solutions slowly, and the mixture was kept overnight until the reactions conducted completely. The products were then washed with ultrapure water and centrifuged twice to remove residual benzene and $KMnO_4$. Finally, the products were dried in the air for the latter use.

### Preparation of the electrode

The composites were mixed with acetylene black (15 wt.%) and dispersed in 0.5 mL of anhydrous ethanol solution by sonication for 5 min. The mixtures were then cast onto a polished glassy carbon electrode and fasten with 2 μL of nafion ethanol solution (1% V/V). The electrodes were dried in the air for latter testing.

### Characterization

The morphology of the sample was characterized by scanning electron microscopy (SEM, JSM-6700 F, JEOL Ltd., Akishima-shi, Japan) at an accelerating voltage of 10 kV. Transmission electron microscope (TEM) micrographs are taken with a JEOL2100 TEM (JEOL Ltd., Akishima-shi, Japan) operating at 200 kV. X-ray diffraction (XRD) patterns were collected using X-ray powder diffraction (XRD, Bruker D8 Advance X-ray diffractometer, Bruker AXS, Inc., Madison, WI, USA; Cu Kα radiation $\lambda$=1.5418 Å) at a scan rate of 0.02 $s^{-1}$. Fourier transform infrared spectroscopy (FTIR) analyses were carried out using a Vertex 70 FTIR spectrophotometer (Bruker AXS, Inc., Madison, WI, USA).

A CHI 760C electrochemical workstation (CHI Instruments, Austin, TX, USA) was used to collect electrochemical data. All electrochemical experiments were conducted in a three-electrode cell, in which a 1.5×1.5 $cm^2$ Pt plate was used as the counter electrode and a saturated calomel electrode was selected as the reference electrode.

## Results and discussion

The schematic of $MnO_2$/PANI fabrication procedure is shown in Figure 1. The reaction commences at the interface of the two solutions immediately as the aniline solution is carefully spread onto the aqueous solution of $KMnO_4$. The interfacial polymerization does not terminate until $KMnO_4$ or aniline is consumed completely. The products diffuse into the aqueous solution spontaneously due to the doping procedure of the polymers and hydrophilic property of hydrate $MnO_2$. The color of the products in different solutions (a to e: 1, 0.5, 0.2, 0.1, and 0 M $HClO_4$, respectively, as shown in the inset of Figure 1) turns from green to brown. This color evolvement is attributed to the different components of composites accompanying with the change of PANI-doping degree. The SEM and TEM images, FTIR spectra, and XRD patterns were employed to investigate the components and the formation of the products.

PANI nanofibers form at the interface between the organic and 1 M$HClO_4$ aqueous solution. As observed in the SEM image (Figure 2), the diameter and length of the nanofibers are around 100 to 200 nm and over 1 μm, respectively. Additionally, it reveals that the nanofibers are twisted and networks are formed by random interconnection, which agrees with the previous reports [3,23,24]. To indicate the evolvement of the samples' morphologies with the changing of acid concentrations, the TEM images of $MnO_2$/PANI fabricated at different acid concentrations are collected in Figure 3. As shown in Figure 3A, PANI nanowires synthesized in 1 M $HClO_4$ solution is consistent with the SEM result in Figure 2. When the interfacial polymerization is carried out using 0.5 M $HClO_4$ (Figure 3B), the conventional nanowire almost disappears. On the contrary, interconnected agglomerating chains appear. In addition, a number of hollow spheres can be observed. Interestingly, when the acid concentration decreases to 0.2 M (Figure 3C), a larger portion of hollow spheres is observed. However, the portion of hollow spheres is decreasing with the decrease of the acid concentrations in the range of 0.1 and 0 M $HClO_4$ (shown in Figure 3D,E,F). In this way, we can modulate the sample structures easily by adjusting the pH of the aqueous solution.

An explanation in the procedure of composite fabrication is proposed in our work. Firstly, aniline monomers

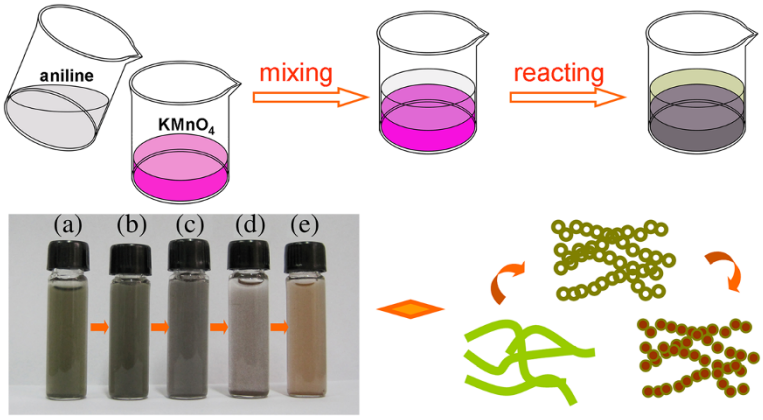


**Figure 1** The schematic of the synthesis procedure and the morphologies of $MnO_2$/PANI composites at different $HClO_4$concentrations.

are polymerized only at the interface of the organic and aqueous phases, so that hydrophilic nanofibers can be separated from the interface and diffuse into the aqueous solution, which prevent the secondary growth and provide space for new nanofiber growing. Additionally, $MnO_2$, as an oxidative regent for PANI polymerization, is used as sacrificial materials in forming various PANI structures [31,32]. According to the change of the morphologies (nanofibers, hollow spheres, and solid particles), it is reasonable to assume that the appearance of the intermediate of $MnO_2$ is a critical role in the formation of hollow spheres. As illustrated in Equations 1 and 2, for the low-acid concentration (0.5, 0.2, and 0.1 M), there is not enough $H^+$ at the interface to resolve the intermediate of $MnO_2$ because of the rapid $H^+$ consumption in the reaction (Equation 2). In the meantime, the resolution of $MnO_2$ restarts while the composite removes from the interface. The consequential reducing reaction of $MnO_2$ follows Equation 3 [33]:

$$MnO_2 + 4H^+ + 2e = Mn^{2+} + 2H_2O \quad (3)$$

In the acid solution of lower concentrations (0.1 and 0 M $HClO_4$), $MnO_2$ appears both at the interface and the bulk solution, which caused a little portion of or no hollow spheres to obtain. In our study, it is thought that large amount of $MnO_2$/PANI composites can be obtained at low-acid concentration, and the $MnO_2$ nanoparticles are wrapped by PANI.

FTIR spectra (Figure 4) were measured to identify the component of the different samples. Among peaks assigned to PANI, the characteristic peaks around 1,580 and 1,497 $cm^{-1}$ relate to the stretching vibration of quinoid (–N=($C_6H_4$)=N-) ring and benzenoid (–($C_6H_4$)-) ring, respectively. Another main band at 1,303 $cm^{-1}$ can be assigned to the stretching of C-N in -NH-($C_6H_4$)-NH-. The bands appeared at 1,143 $cm^{-1}$ and 829 $cm^{-1}$ which correspond to the stretching of C-H in-plane and C-H out-of-plane bendings. In addition, the bands of N-H (PANI) and O-H ($H_2O$) at 3,230 and 3,400 $cm^{-1}$, respectively, are observed. As noticed, the band near 3,400 $cm^{-1}$ (O-H) is becoming intense with the decrease of the acid concentration, which is attributed to the appearance of hydrate $MnO_2$. The above conclusion is proved by the annealing experiments: the band at 3,400 $cm^{-1}$ (O-H) of hydrate $MnO_2$ vanished after 500°C heat treatment (Additional file 1: Figure S1). The band near 1,303 $cm^{-1}$ is becoming weaker from curves g to a in Figure 4, which suggests that the doping degree of PANI is changing with the acid concentration. The characteristic bands of curves a, b, and c in Figure 4 shifted right compared with the others, which is ascribed to the effect of $MnO_2$ on PANI. It demonstrates that

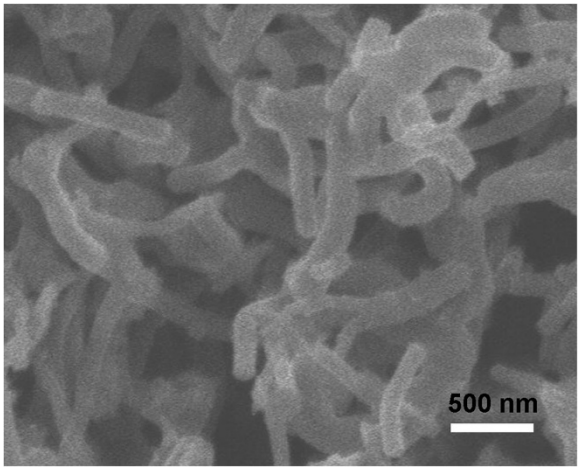


**Figure 2** SEM images of PANI synthesized by interfacial polymerization at 1 M $HClO_4$.

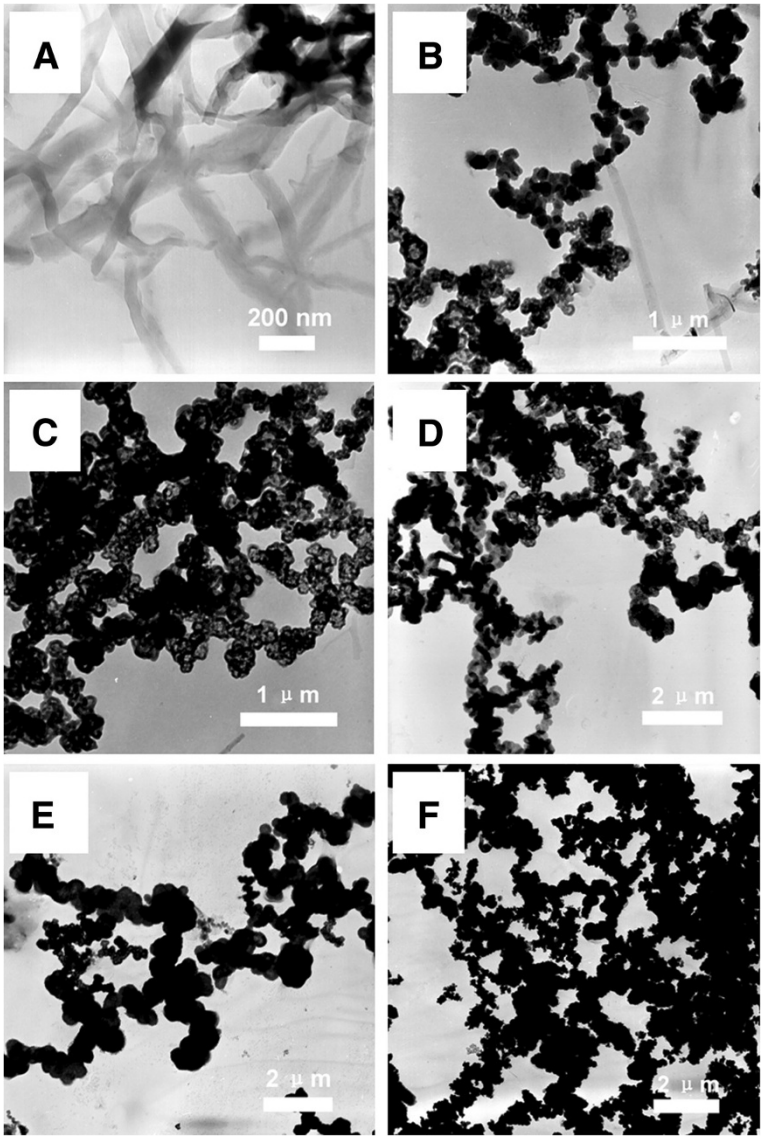


**Figure 3 TEM images of $MnO_2$/PANI composites synthesized at different acid concentrations.** (**A**) 1, (**B**) 0.5, (**C**) 0.2, (**D**) 0.1, (**E**) 0.05, and (**F**) 0 M $HClO_4$.

some special interaction exists between $MnO_2$ and PANI.

Due to the ordered and metallic-like property, conducting polymers possess particular crystallinity and orientation. As shown in the XRD patterns in Figure 5A, there are no identified peaks appeared for the products synthesized in low-acid concentrations (curves a to e: 0.1 M NaOH, and 0, 0.02, 0.05, and 0.1 M $HClO_4$, respectively), which indicates the products are amorphous. For the products obtained at 0.2 (curve f), 0.5 (curve g), and 1 M $HClO_4$ (curve h), two intense XRD peaks $2\theta \approx 20$ and 25° are observed corresponding to pure PANI according to previous literature [2]. All above results confirm that the crystallized PANI can be formed at higher acid concentrations in this work.

To further analyze the components at different acid concentrations, the samples were treated at 500°C (at which $MnO_x$ is crystallizing and PANI will be burned). The products obtained at 1, 0.5, and 0.2 M $HClO_4$ were burned out with no solids left, which indicates that there is no $MnO_2$ generating at such acid concentrations. Contrary to higher acid concentration, the solid residue of the products obtained at 0.1, 0.05, 0.02, and 0 M $HClO_4$ turned black. The FTIR spectra of the heat-treated composites fabricated in 0.1, 0.05, 0.02, and 0 M $HClO_4$ were measured (Additional file 1: Figure S2). The

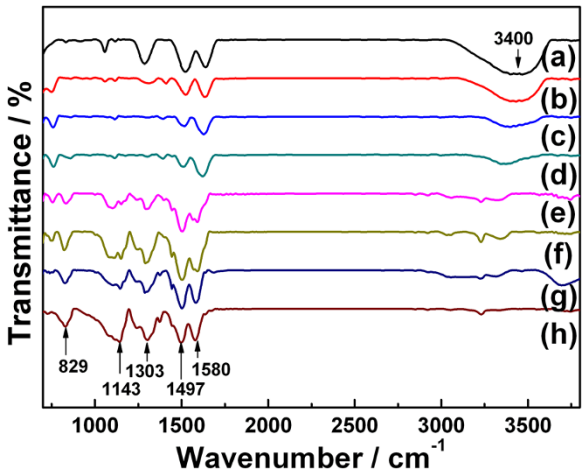


**Figure 4 FTIR spectra of the as-prepared samples.** Curves a to g: $MnO_2$/PANI fabricated in 0, 0.02, 0.05, 0.1, 0.2, 0.5, and 1 M $HClO_4$, respectively.

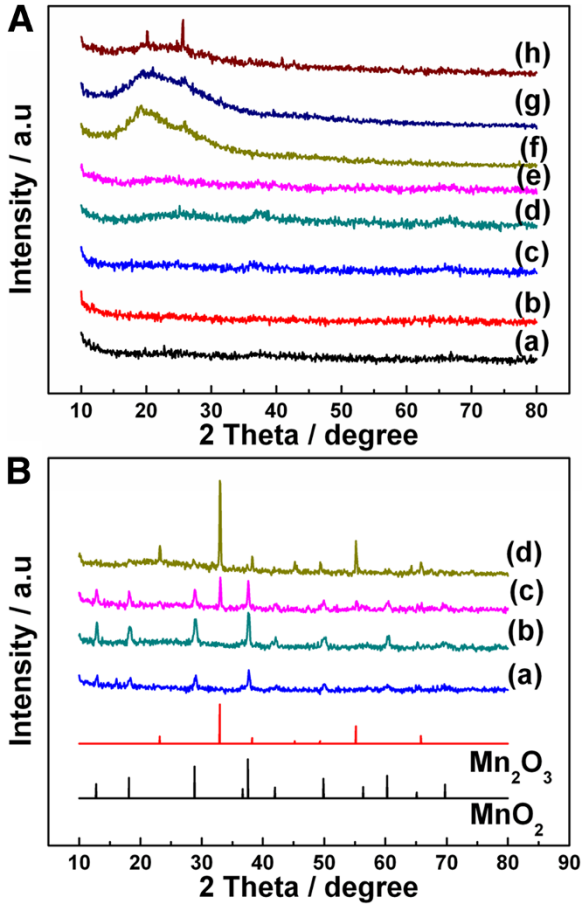


**Figure 5 XRD patterns of the samples.** (**A**) The XRD patterns of the composites, curves a to h: $MnO_2$/PANI fabricated in 0.1 M NaOH and 0, 0.02, 0.05, 0.1, 0.2, 0.5, and 1 M $HClO_4$, respectively. (**B**) XRD pattern of the samples, curves a to d: annealed $MnO_2$/PANI fabricated in 0, 0.02, 0.05, and 0.1 M $HClO_4$, respectively.

characteristic FTIR spectra bands of PANI vanish after heat treatment, which confirms that PANI has been pyrolyzed after heat treatment.

The XRD patterns of the samples after heat treatment are shown in Figure 5B. The XRD patterns of the composite obtained in 0 (curve a) and 0.02 M $HClO_4$ (curve b) can be indexed to $\alpha$-$MnO_2$ crystal structures [34]. Meanwhile, different XRD peaks are observed in Figure 5B (curves c and d), indicating the heat-treated product obtained in 0.1 M $HClO_4$ is $Mn_2O_3$ and the heat-treated product obtained in 0.05 M $HClO_4$ are $MnO_2$ and $Mn_2O_3$. The results show that for as-prepared samples, $Mn_2O_3$ phase is increasing with acid concentration. It is reported that the phase of manganese oxides is changing with temperature, and $MnO_2$ may transform to suboxide $Mn_2O_3$ at 500°C to 900°C [33,35-38]. The reductive matters such as $CH_3OH$, $CH_4$, and CO were studied as reductions for the phase transforming of $MnO_2$ to $Mn_2O_3$, and the mechanism was also suggested [34,39]. Therefore, we assume that the reductive matters generated during PANI decomposition procedure assists the transformation of $MnO_2$ to $Mn_2O_3$. Additionally, the aggravating degree of phase transforming of the heat-treated samples could be attributed to the increasing proportion of PANI in the composites. All the above results indicate that the $MnO_2$ generated in the polymerization of PANI process at low-acid concentration has a great effect on the formation of the hollow structure at higher acid concentrations as an intermediate.

In this work, the electrochemical performance of the composite was evaluated. The capacitance of $MnO_2$ is generated by the charge transferring among multivalent Mn element ($Mn^{2+}$, $Mn^{3+}$, $Mn^{4+}$, and $Mn^{6+}$) [35], while PANI endures doping/dedoping companying with the redox process of PANI:

$$[\mathrm{PANI}^0] + \mathrm{A}^- \rightarrow [\mathrm{PANI}^+]\,\mathrm{A}^- + e^- \quad (4)$$

$$[\mathrm{PANI}^+]\,\mathrm{A}^- + e^- \rightarrow [\mathrm{PANI}^0] + \mathrm{A}^- \quad (5)$$

Cyclic voltammetry (CV) curves of the composites are shown in Figure 6A. CV curves of as-prepared PANI nanofibers/$MnO_2$ crystallines are comparable with pure PANI and $MnO_2$, respectively. The rectangle-like shape of CV curve suggests that $MnO_2$/PANI fabricated in 0.02 M $HClO_4$ has an ideal capacitive characterization. Additionally, the rectangle-like shape potential region of $MnO_2$/PANI (curve c) is relatively larger compared with that of the crystallized $MnO_2$ (curve e) and PANI (curve a). The capacitance $C_{CP}$ can be estimated according to the equation: $C_{CP} = (Q_a + Q_c)/(2 \times \Delta V)$, where $Q_a$, $Q_c$, and $\Delta V$ are indicative of the anodic and cathodic charges of CV and the potential region of CV, respectively. The

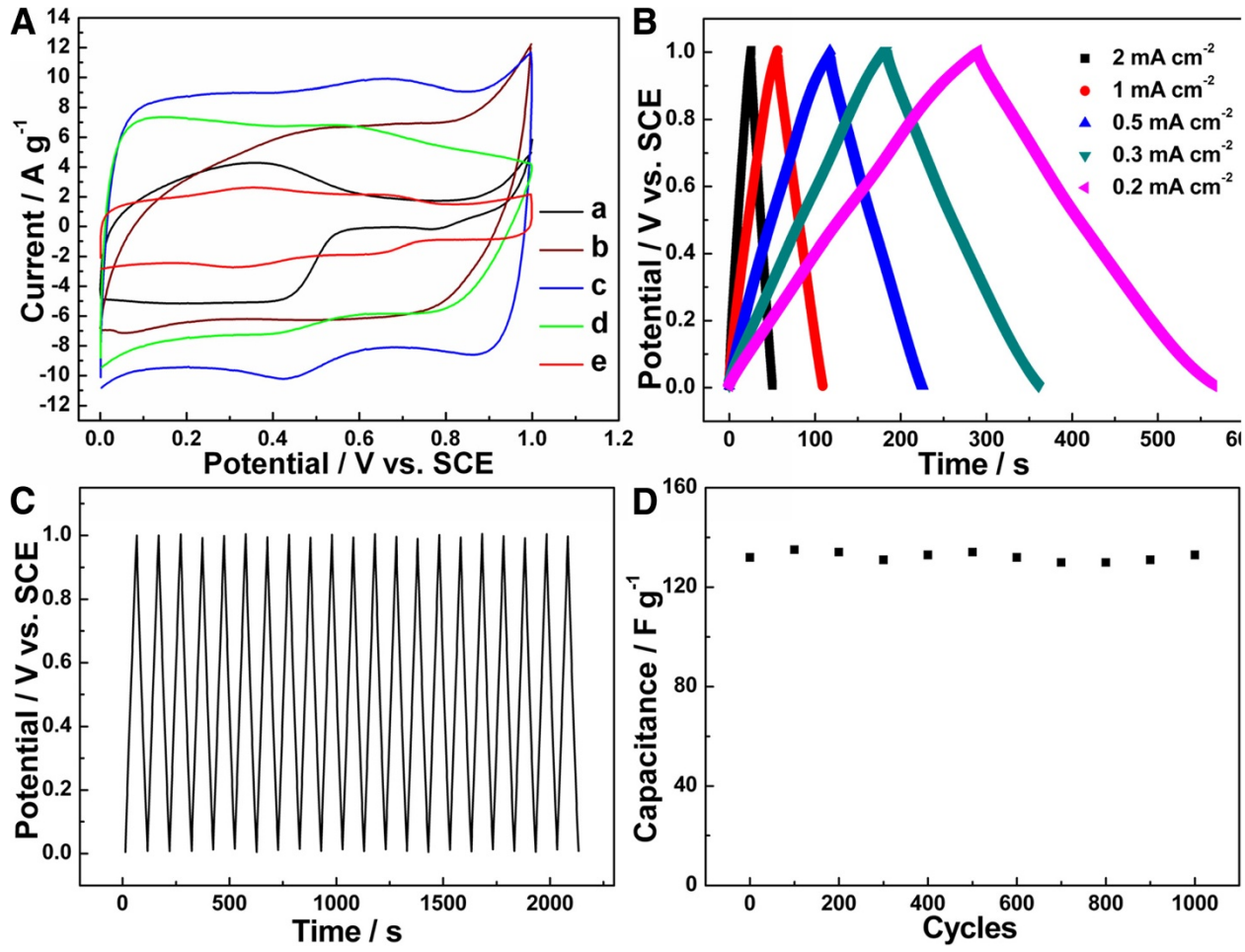


**Figure 6 CV and charge–discharge curves of the composites.** (**A**) CV curves of the as-prepared samples in 0.1 M $HClO_4$solution at 50 mV $s^{-1}$, curves a to d: $MnO_2$/PANI fabricated in 1, 0.05, and 0.02 M $HClO_4$, and 0.1 M NaOH, respectively. Curve e: 500°C-treated $MnO_2$/PANI fabricated in 0.02 M $HClO_4$. (**B**) Charge–discharge curves of the $MnO_2$/PANI composite in 0.1 M $HClO_4$ solution at different current densities. (**C**) First 20 cycles of charge–discharge curves for the $MnO_2$/PANI composite at the current density of 1 mA $cm^{-2}$ (**D**) Dependence of capacitance of the $MnO_2$/PANI composite on the charge–discharge cycles at the current density of 1 mA $cm^{-2}$.

capacitances of the samples in curves a to e are 80, 45, 207, 143, and 46 F $g^{-1}$, respectively. The capacitance of $MnO_2$/PANI (curve c) is larger than that of PANI (curve a) and $MnO_2$ (curve e). The extended ideal capacitive potential region and larger capacitance of $MnO_2$/PANI composite are possibly due to the synergistic effect between the core of $MnO_2$ and the shell of PANI [32,35,40].

The charge–discharge curves of $MnO_2$/PANI fabricated in 0.02 M $HClO_4$ were measured at various current densities (shown in Figure 6B). The E-t plots show symmetry, which indicate the reversible charge–discharge process of the $MnO_2$/PANI composite. The specific capacitance of the sample can be calculated via the equation: $C_{CP} = i/|dE/dt|$, where $|dE/dt|$ is estimated from the slope of the discharging curves. The capacitance of the composite at 2, 1, 0.5, 0.3, and 0.2 mA $cm^{-2}$ achieves 159, 161, 170, 174, and 168 F $g^{-1}$, respectively. Additionally, the discrepancy of the largest composite capacitance values estimated from discharging and CV curves is lower than 20%, which suggests the high credibility of both techniques.

The stabilities of the samples were tested with 100 CV scan cycles (Additional file 1: Figure S3). After 100 cycles, the CV curves of PANI change obviously and the capacitances decreased largely (Additional file 1: Figure S3 A, B). However, with the increase of $MnO_2$, the CV curves change a little and even no capacitance decrease is observed (as shown in Additional file 1: Figure S3 C,D,E). Compared with PANI samples obtained at higher acid concentration, $MnO_2$/PANI nanocomposites possess noticeable capacitive stability. To investigate the long-term stability of as-prepared $MnO_2$/PANI nanocomposites, the charge–discharge test of 1,000 cycles was conducted at 1 mA $cm^{-2}$ in 0.1 M $HClO_4$. As shown in Figure 6C (first 20 cycles are shown for clearly observation), the E-t plots are symmetric

in shape and have almost no change during the long-term test. From Figure 6D, it can be seen that the discrepancy of capacitance of $MnO_2$/PANI during 2,000-cycle test is lower than 5%, and there is no evident capacitance decrease after 1,000 cycles. The stability of the $MnO_2$/PANI composite is thought due to the protection of the shield-surrounded PANI and uniform dispersion of $MnO_2$ particles, whereby avoiding severe particles conglomeration involved in the charge–discharge process [35,36]. The facile synthesis and ideal electrochemical capacitive performance will probably give the composites a promising prospect in the application of supercapacitors.

## Conclusions

A series of samples including $MnO_2$/PANI composites and PANI nanofibers were successfully synthesized by the facile interfacial polymerization. Controllable and uniform synthesis of the composites has been realized by simply adjusting the pH of the solution. The effect of acid concentration and the related mechanism of the formation of the products are investigated. We demonstrate that the intermediate of $MnO_2$ plays a key role in forming the hollow structures of PANI. The capacitance of the composite achieves 207 F $g^{-1}$, and the results suggest that the $MnO_2$/PANI composites show superior performance over pure PANI or $MnO_2$.

## Additional file

**Additional file 1: Figure S1.** FTIR spectra of $MnO_2$/PANI fabricated in 0.1 M NaOH, 0 $HClO_4$, 0.02 M. **Figure S2.** FTIR spectra of polyaniline (curve a) and the composites after heat treatment (curves b to f): $MnO_2$/PANI fabricated in 0.1 M NaOH, and 0, 0.02, 0.05, and 0.1 M $HClO_4$. **Figure S3.** CV curves of the composites before and after 100 cycles stability tests in 0.1 M $HClO_4$ solution at 50 mV $s^{-1}$, (**A-D**) samples fabricated in 1, 0.05, and 0.02 M $HClO_4$, and 0.1 M NaOH and (**E**) $MnO_2$ obtained by heating $MnO_2$/PANI composite fabricated in 0.02 M $HClO_4$.

#### Competing interests

The authors declare that they have no competing interests.

#### Authors' contributions

FM carried out the total experiment and wrote the manuscript. XY participated in the detection of the SEM and TEM. YZ participated in the data analysis. PS participated in the design of the experiment and performed the data analysis. All authors read and approved the final manuscript.

#### Acknowledgements

This work was supported by the National Basic Research Program of China (2012CB932800) and the National Science Foundation of China (51171092, 20906045, 90923011). The authors also thank the Shandong University for their financial support (nos.31370056431211, 31370070614018, and 31370056431211).

#### Author details

[1]Key Laboratory for Liquid–solid Structural Evolution and Processing of Materials, Ministry of Education, School of Materials Science and Engineering, Shandong University, Jinan 250061, People's Republic of China. [2]School of Chemistry and Chemical Engineering, Shandong University, Jinan 250100, People's Republic of China. [3]School of Chemistry and Bioscience, Ili Normal University, Xinjiang 835000, People's Republic of China.

Received: 5 February 2013 Accepted: 4 March 2013
Published: 17 April 2013

#### References

1. Wang K, Huang J, Wei Z: **Conducting polyaniline nanowire arrays for high performance supercapacitors.** *J Phys Chem C* 2010, **114:**8062–8067.
2. Zhang K, Zhang LL, Zhao XS, Wu J: **Graphene/polyaniline nanofiber composites as supercapacitor electrodes.** *Chem Mater* 2010, **22:**1392–1401.
3. Huang J, Virji S, Weiller BH, Kaner RB: **Polyaniline nanofibers: facile synthesis and chemical sensors.** *J Am Chem Soc* 2003, **125:**314–315.
4. McQuade DT, Pullen AE, Swager TM: **Conjugated polymer-based chemical sensors.** *Chem Rev* 2000, **100:**2537–2574.
5. Li D, Huang J, Kaner RB: **Polyaniline nanofibers: a unique polymer nanostructure for versatile applications.** *Acc Chem Res* 2009, **42:**135–145.
6. Athouel L, Moser F, Dugas R, Crosnier O, Belanger D, Brousse T: **Variation of the $MnO_2$ birnessite structure upon charge/discharge in an electrochemical supercapacitor electrode in aqueous $Na_2SO_4$electrolyte.** *J Phys Chem C* 2008, **112:**7270–7277.
7. Devaraj S, Munichandraiah N: **Effect of crystallographic structure of $MnO_2$ on its electrochemical capacitance properties.** *J Phys Chem C* 2008, **112:**4406–4417.
8. Qu QT, Zhang P, Wang B, Chen YH, Tian S, Wu YP, Holze R: **Electrochemical performance of $MnO_2$ nanorods in neutral aqueous electrolytes as a cathode for asymmetric supercapacitors.** *J Phys Chem C* 2009, **113:**14020–14027.
9. Benedetti TM, Bazito FFC, Ponzio EA, Torresi RM: **Electrostatic layer-by-layer deposition and electrochemical characterization of thin films composed of $MnO_2$ nanoparticles in a room-temperature ionic liquid.** *Langmuir* 2008, **24:**3602–3610.
10. Downs C, Nugent J, Ajayan PM, Duquette DJ, Santhanam KSV: **Efficient polymerization of aniline at carbon nanotube electrodes.** *Adv Mater* 1999, **11:**1028–1031.
11. Long JW, Sassin MB, Fischer AE, Rolison DR: **Multifunctional $MnO_2$-carbon nanoarchitectures exhibit battery and capacitor characteristics in alkaline electrolytes.** *J Phys Chem C* 2009, **113:**17595–17598.
12. Chen S, Zhu J, Wu X, Han Q, Wang X: **Graphene oxide-MnO $_2$nanocomposites for supercapacitors.** *ACS Nano* 2010, **4:**2822–2830.
13. Cuentas-Gallegos AK, Gomez-Romero P: **In-situ synthesis of polypyrrole-$MnO_{2-x}$nanocomposite hybrids.** *J New Mat Electrochem Systems* 2005, **8:**181–188.
14. Li GR, Feng ZP, Ou YN, Wu D, Fu R, Tong YX: **Mesoporous $MnO_2$/carbon aerogel composites as promising electrode materials for high-performance supercapacitors.** *Langmuir* 2010, **26:**2209–2213.
15. Wang LC, Liu YM, Chen M, Cao Y, He HY, Fan KN: **$MnO_2$nanorod supported gold nanoparticles with enhanced activity for solvent-free aerobic alcohol oxidation.** *J Phys Chem C* 2008, **112:**6981–6987.
16. Gemeay AH, El-Sharkawy RG, Mansour IA, Zaki AB: **Catalytic activity of polyaniline/$MnO_2$composites towards the oxidative decolorization of organic dyes.** *Appl Catal B: Environ* 2008, **80:**106–115.
17. Gemeay AH, El-Sharkawy RG, Mansour IA, Zaki AB: **Preparation and characterization of polyaniline/manganese dioxide composites and their catalytic activity.** *J Colloid Interface Sci* 2007, **308:**385–394.
18. Razak SIA, Ahmad AL, Zein SHS, Boccaccini AR: **$MnO_2$-filled multiwalled carbon nanotube/polyaniline nanocomposites with enhanced interfacial interaction and electronic properties.** *Scripta Mater* 2009, **61:**592–595.
19. Liu FJ: **One-step synthesis of $MnO_2$particles distributed polyaniline–poly (styrene-sulfonic acid).** *Synth Met* 2009, **159:**1896–1899.
20. Sathish M, Mitani S, Tomai T, Honma I: **$MnO_2$ assisted oxidative polymerization of aniline on graphene sheets: Superior nanocomposite electrodes for electrochemical supercapacitors.** *J Mater Chem* 2011, **21:**16216–16222.
21. Chaudhuri RG, Paria S: **Core/shell nanoparticles: classes, properties, synthesis mechanisms, characterization, and applications.** *Chem Rev* 2012, **112:**2373–2433.
22. Saha K, Agasti SS, Kim C, Li X, Rotello VM: **Gold nanoparticles in chemical and biological sensing.** *Chem Rev* 2012, **112:**2739–2779.
23. Huang J, Kaner RB: **A general chemical route to polyaniline nanofibers.** *J.AmChem Soc* 2004, **126:**851–855.
24. Huang J, Kaner RB: **Nanofiber formation in the chemical polymerization of aniline: a mechanistic study.** *Angew Chem Int Ed* 2004, **43:**5817–5821.
25. Miller JR, Simon P: **Electrochemical capacitors for energy management.** *Science* 2008, **321:**651.

26. Simon P, Gogotsi Y: **Materials for electrochemical capacitors.** *Nature Mater* 2008, **7:**845.
27. Ni WB, Wang DC, Huang ZJ, Zhao JW, Cui G: **Fabrication of nanocomposite electrode with $MnO_2$ nanoparticles distributed in polyaniline for electrochemical capacitors.** *Mater Chem Phys* 2010, **124:**1151–1154.
28. Yuan CZ, Su LH, Gao B, Zhang XG: **Enhanced electrochemical stability and charge storage of $MnO_2$/carbon nanotubes composite modified by polyaniline coating layer in acidic electrolytes.** *Electrochim Acta* 2008, **53:**7039–7047.
29. Li Q, Liu JH, Zou JH, Chunder A, Chen YQ, Zhai L: **Synthesis and electrochemical performance of multi-walled carbon nanotube/polyaniline/$MnO_2$ternary coaxial nanostructures for supercapacitors.** *J Power Sources* 2011, **196:**565–572.
30. MacDiarmid AG, Jones WE, Norris ID, Gao J, Johnson AT, Pinto NJ, Hone J, Han B, Ko FK, Okuzaki H, Llaguno M: **Electrostatically-generated nanofibers of electronic polymers.** *Synth Met* 2001, **119:**27–30.
31. He HX, Li CZ, Tao N: **Conductance of polymer nanowires fabricated by a combined electrodeposition and mechanical break junction method.** *J Appl Phys Lett* 2001, **78:**811–813.
32. Pan LP, Pu L, Shi Y, Song SY, Xu Z, Zhang R, Zheng YD: **Synthesis of polyaniline nanotubes with a reactive template of manganese oxide.** *Adv Mater* 2007, **19:**461–464.
33. Yuan ZY, Zhang Z, Du G, Ren TZ, Su BL: **A simple method to synthesise single-crystalline manganese oxide nanowires.** *Chem Phys Lett* 2003, **378:**349–353.
34. Liang S, Teng F, Bulgan G, Zong R, Zhu Y: **Effect of phase structure of $MnO_2$nanorod catalyst on the activity for CO oxidation.** *J Phys Chem C* 2008, **112:**5307–5315.
35. Craciun R, Dulamita N: **Influence of $La_2O_3$promoter on the structure of$MnO_x$/$SiO_2$catalysts.** *Catal Lett* 1997, **46:**229–234.
36. Kim SH, Kim SJ, Oh SM: **Preparation of layered $MnO_2$via thermal decomposition of $KMnO_4$and its electrochemical characterizations.** *Chem Mater* 1999, **11:**557–563.
37. Wang N, Cao X, He L, Zhang W, Guo L, Chen C, Wang R, Yang S: **One-pot synthesis of highly crystallined β-$MnO_2$nanodisks assembled from nanoparticles: morphology evolutions and phase transitions.** *J Phys Chem C* 2008, **112:**365–369.
38. Luo J, Zhu HT, Fan HM, Liang JK, Shi HL, Rao GH, Li JB, Du ZM, Shen ZX: **Synthesis of single-crystal tetragonal α-$MnO_2$nanotubes.** *J Phys Chem C* 2008, **112:**12594–12598.
39. Stobbe ER, Boer BA, Geus JW: **The reduction and oxidation behaviour of manganese oxides.** *Catal Today* 1999, **47:**161–167.
40. Ballav N: **High-conducting polyaniline via oxidative polymerization of aniline by $MnO_2$, $PbO_2$and $NH_4VO_3$.** *Mater Lett* 2004, **58:**3257–3260.

doi:10.1186/1556-276X-8-179
**Cite this article as:** Meng *et al.*: Controllable synthesis of $MnO_2$/polyaniline nanocomposite and its electrochemical capacitive property. *Nanoscale Research Letters* 2013 **8**:179.